Sub-Terahertz Frequency-Domain Spectroscopy Reveals Single-Grain Mobility and Scatter Influence of Large-Area Graphene

*Christian Cervetti, Eric Heintze, Boris Gorshunov, Elena Zhukova, Svyatoslav Lobanov, Alexander Hoyer, Marko Burghard, Klaus Kern, Martin Dressel, and Lapo Bogani**

Graphene,[1] a 2D hexagonal crystal of carbon atoms, attracts immense interest owing to its extraordinary properties and potential applications, ranging from stretchable[2] and transparent electronics[3] to biosensors[4] and spintronics.[5] While most fundamental studies have been performed on micrometer-size single flakes[1] cleaved from graphite, many applications require wafer-sized graphene layers[2,6] on various substrates.[7,8] Increasing effort is thus being devoted to the fabrication and characterization of large-area graphene, whose properties however differ significantly from those of its "clean" small-flake counterparts.[9] In particular, grain boundaries,[10] defects,[11] ripples,[12] and growth leftovers influence its electronic behavior. As a consequence, broadly varying electronic quality has been reported, as reflected for example in a carrier mobility range[7,13–15] from 100 to 45 000 $cm^2\ s^{-1}\ V^{-1}$. Identifying the major factors that govern the structural and electronic quality of large area graphene is hence of great importance for its technological implementation.

Chemical vapor deposition (CVD) on transition metal substrates (e.g., Cu or Ni) has become one of the most promising production methods for wafer-sized graphene, providing sheets up to 30 inches long[16] transferable onto different substrates.[17] A major factor that limits the quality of CVD graphene is the presence of metallic residues from the underlying substrate, mostly in the form of micro- and nanosized particles.[18,19] As such leftovers can influence the performance of the final devices,[20] protocols have been developed to yield reasonably clean CVD graphene. In this regard, low-energy optical techniques have recently emerged as powerful tool to study fundamental phenomena in graphene,[21] such as, excited carrier dynamics by pump-probe experiments[22–24] and time-domain spectroscopy,[25,26] Dirac fermion behavior using Fourier transform IR spectroscopy[19,27–29] and the effect of substrate,[30] and doping[31,32] on the graphene optical response.

Despite this progress, the correlation between residual metal contaminants and the electronic quality of graphene is still unclear. Here we address this issue by performing quasi-optical sub-terahertz (sub-THz) spectroscopy to detect the presence of sub-micrometer conducting contaminants in CVD graphene. We show that this technique provides direct access to the optical conductivity of graphene, with the high accuracy necessary for probing the subtle influence of a low density of metal residues. Moreover, it can be easily expanded to gated structures to extract the intrinsic electronic properties of individual graphene domains such as carrier mobility, enabling us to identify the limiting scattering mechanisms in a contactless fashion.

Commercially available CVD graphene on copper was transferred onto ultrapure Si and crystalline Al_2O_3 substrates, both with a lateral size of 1 cm^2 and a thickness of 500 µm. These substrates are suitable for graphene-based solar cells and detectors, and highly transparent to THz and far-IR radiation. The employed transfer process, **Figure 1**a, starts with the deposition of a poly(methyl methacrylate) (PMMA) layer onto the Cu/graphene by spin coating. The copper foil is removed by placing the Cu/Graphene/PMMA stack on the etching solution surface for a time t_{etch} at room temperature (see Methods). To remove residual etchant, the stack is immersed for 1 h in dilute HCl, and then transferred into a deionized water bath. The graphene/PMMA bilayer is then picked up from the bottom by the desired substrate. Slow drying on a hotplate at 50 °C minimized ruptures in the graphene membrane, while subsequent annealing at 160 °C for 2 h ensured a smoother film surface. Finally, the PMMA layer was removed by consecutive soaking in organic solvents (Methods). After PMMA removal, the graphene layer still covers the whole sample area (Figure 1b). It exhibits some fractures and folds typical of CVD graphene. The presence of copper contaminants, whose size and abundance depend on t_{etch}, is clearly visible.

The graphene films were investigated by micro-Raman spectroscopy (Figure 1c). The Raman 2D peak at 2700 cm^{-1}, associated with the second order zone boundary phonons, is sensitive to the number of graphene layers.[33] For the present samples, the 2D

C. Cervetti, E. Heintze, Prof. B. Gorshunov, Dr. E. Zhukova, Prof. M. Dressel, Dr. L. Bogani[+]
1. Physikalisches Institut
Universität Stuttgart
Pfaffenwaldring 57, D-70550 Stuttgart, Germany
E-mail: lapo.bogani@materials.ox.ac.uk
Prof. B. Gorshunov, Dr. E. Zhukova, S. Lobanov
Moscow Institute of Physics and Technology (State University)
Institutskii Pereulok 9, Dolgoprudny, Moscow Region, Russia
Prof. B. Gorshunov, Dr. E. Zhukova, S. Lobanov
Prokhorov General Physics Institute
Russian Academy of Sciences
Vavilov str. 38, 119991 Moscow, Russia
A. Hoyer, Dr. M. Burghard, Prof. K. Kern
Max Planck Institut für Festkörperforschung
Heisenbergstrasse 1, D-70569 Stuttgart, Germany
Prof. K. Kern
Institute de Physique de la Matière Condensée
Ecole Polytechnique de Lausanne
1015 Lausanne, Switzerland
[+]Present Address: Department of Materials, University of Oxford, 16 Parks Road, Oxford, OX1 3PH, United Kingdom

DOI: 10.1002/adma.201500599

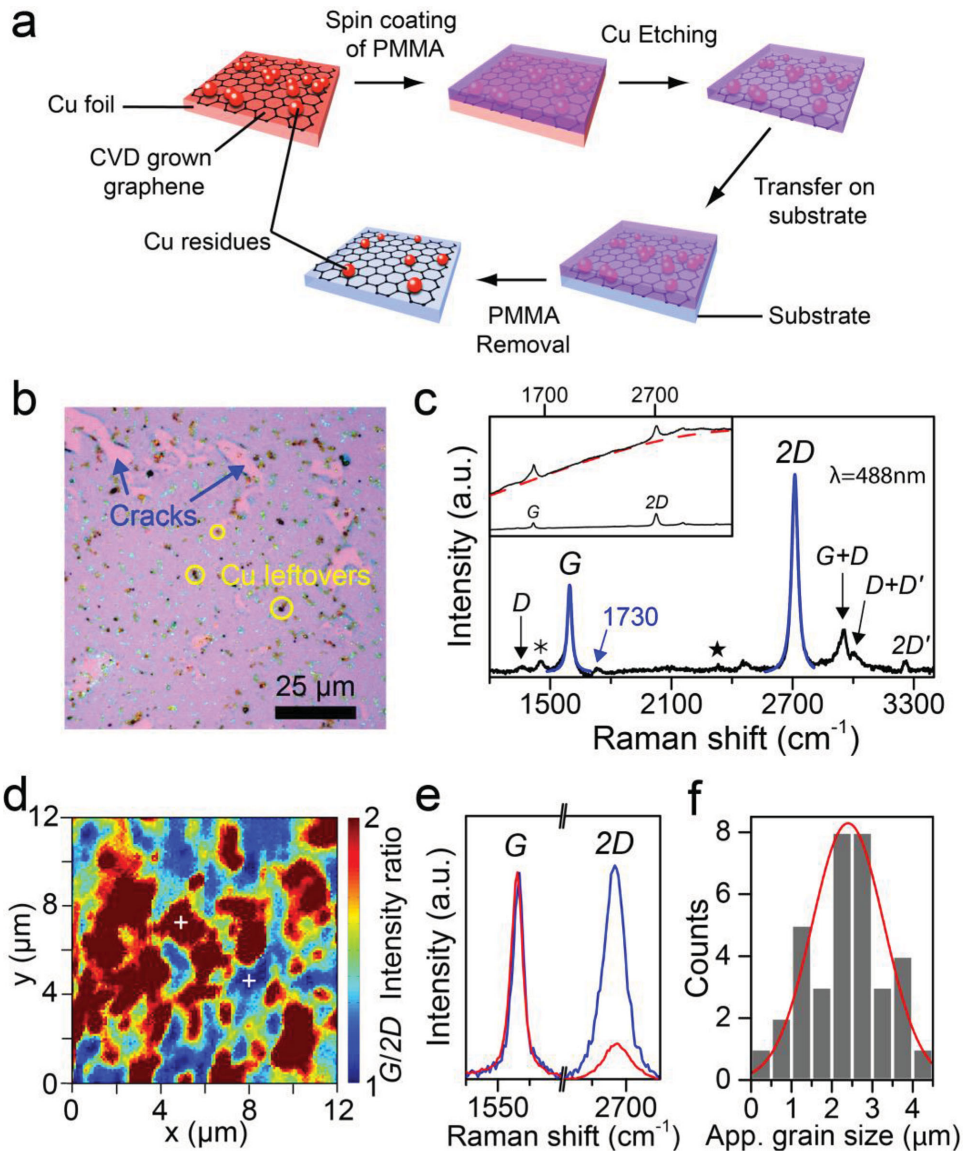

Figure 1. Crystalline quality of transferred CVD graphene. a) Transfer procedure. b) Optical picture of CVD graphene on SiO_2 after 15 min of Cu etching. c) Raman spectrum of graphene on SiO_2. The blue lines are fits with a single Lorentz function. The asterisk and star symbols indicate SiO_2 TO phonon mode and ambient N_2, respectively. Inset: Spectra at different sample positions revealing a variable luminescence background due to Cu leftovers. d) Raman map of the G/2D intensity ratio of a two-layers graphene stack. e) Raman spectra, as acquired at the positions of the white crosses in (d). f) Statistical analysis of the apparent grain lateral size extracted from (d). The red solid line is a fit with Gaussian function.

peak can be fitted with a single Lorentzian function, confirming the presence of single-layer graphene. A G peak, due to the doubly degenerate zone-center E_{2g} phonon, is detected at 1596 cm^{-1}, and its upshift of 16 cm^{-1} indicates moderate doping,[34] corresponding to a residual carrier density of $\approx 10^{12}$ cm^{-2}. The very weak D peak at 1350 cm^{-1}, related to the activation of to the A_{1g} breathing mode at the Brillouin zone boundary by lattice defects, indicates very little disorder and gives rise to additional combined modes in the upper part of the spectrum. A small peak at ≈1730 cm^{-1} is typical of C=O stretching in PMMA residues.[35] Raman spectra acquired at different positions exhibit a variable background photoluminescence testifying the presence of Cu residues,[36] (inset Figure 1c) as also confirmed by scanning electron microscopy (Supporting Information).

CVD graphene, grown on polycrystalline Cu foil, is composed of high quality crystalline grains with random crystallographic orientation.[18] One way to reveal the CVD grain structure is to exploit the Raman intensity dependence on the twist angle in a stacked two layers graphene system.[37] The different crystallographic orientations between the top and bottom layers modulate the interlayer interaction between the domains. On this basis, monitoring the spatial distribution of the G/2D intensity ratio, enables probing the grain structure (Figure 1d,e). Statistical analysis (Figure 1e) yields an apparent grain size distribution peaked at 2.40 ± 0.13 μm corresponding to a mean grain size of ≈5 μm for the single layer.

For the optical investigations, we used a Mach–Zehnder interferometer-based spectrometer[38] (**Figure 2**a) comprising

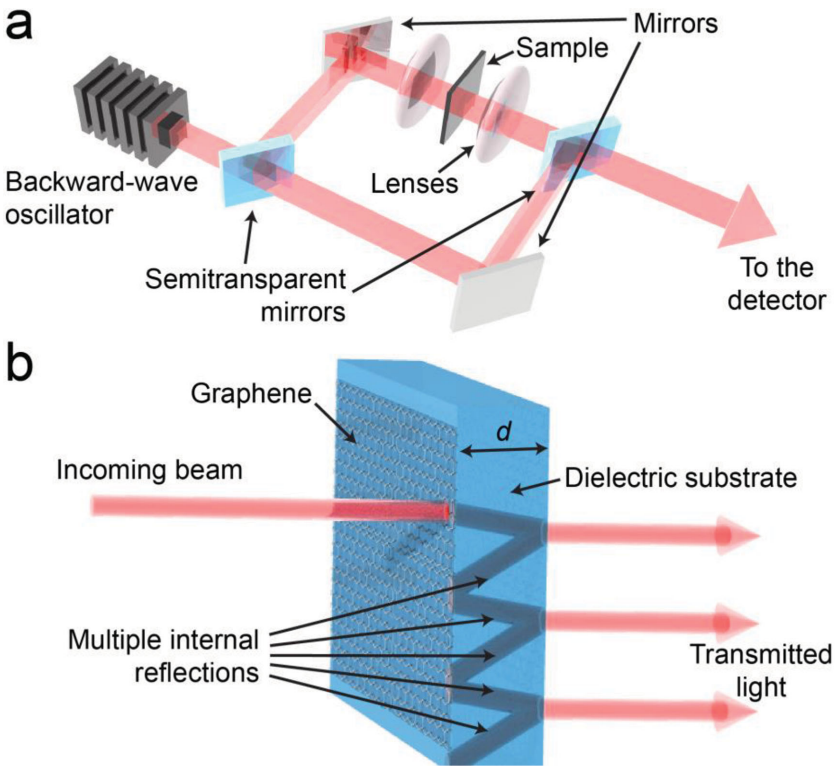

Figure 2. a) Scheme of sub-THz spectrometer. b) Scheme of the multiple internal reflections within the dielectric that lead to Fabry–Perot interferences.

backward-wave oscillators[38] as coherent sources of continuous sub-THz radiation. Their frequency can be continuously tuned between 0.03 and 1.5 THz (corresponding to 1–50 cm^{-1} or 6–0.1 meV). The radiation is detected by either Golay cells or ^{4}He-cooled Si bolometers. The frequency resolution $\Delta\nu/\nu$ is better than 10^{-5}, and the dynamic range is between 40 and 50 dB. The Mach–Zehnder interferometric configuration enabled detecting both amplitude and phase shift of the transmitted radiation, thus opening the possibility to determine the complex electromagnetic response of graphene without involving Kramers–Kronig relations.[39] A round aperture sets the beam diameter to 5 mm, so that several graphene domains are homogeneously irradiated.

The plane-parallel undoped Si or Al_2O_3 substrates implemented a Fabry–Perot resonator formed by the graphene–substrate and substrate–air interfaces (Figure 2b). The resulting multiple reflections allow maximizing the interaction of sub-THz radiation with graphene, and thus to significantly enhance the sensitivity, as in all cavity-based techniques. The electrodynamic response of the resulting multilayer system was analyzed using the Fresnel formulas,[39] according to which the complex transmission $\hat{t}_{ij}$ and reflection $\hat{r}_{ij}$ coefficients at each interface are given by:

$$\hat{t}_{ij} = \frac{\hat{n}_i - \hat{n}_j}{\hat{n}_i + \hat{n}_j}, \hat{r}_{ij} = \frac{2\hat{n}_i}{\hat{n}_i + \hat{n}_j} \quad (1)$$

where i and j are the material indices, and $\hat{n}_i = n_i + ik_i$ the complex refractive indexes (n_i and k_i are the refraction and extinction indexes, respectively). Phase shift and attenuation are described by $e^{i\delta_i}$ terms where $\delta_i = \hat{n}_i d_i c/\omega$, $\omega = 2\pi c\nu$ is the radiation frequency, d_i is the i-layer thickness, and c the light velocity. For air, $n_1 = n_4 = 1$ and $k_1 = k_4 = 0$, while for the dielectric substrate, n_3, k_3, and the thickness d_3 are determined beforehand. The total $\hat{t}$ can thus be written as:[38,39]

$$\hat{t} = \frac{\hat{t}_{12}\hat{t}_{23}\hat{t}_{34}e^{i(\delta_2+\delta_3)}}{1+\hat{r}_{23}\hat{r}_{34}e^{2i\delta_3}}\left(1+\hat{r}_{12}\frac{\hat{r}_{23}+\hat{r}_{34}e^{2i\delta_3}}{1+r_{23}r_{34}e^{2i\delta_3}}e^{2i\delta_2}\right)^{-1} \quad (2)$$

with the measured transmission coefficient $Tr = |t|^2$.

Figure 3a compares the frequency dependence of the transmission coefficient for the bare Si substrate and four graphene samples transferred under the same conditions. Thickness and refractive index of the dielectric substrate[31] determine the period of the interferometric fringes, while the amplitude of the maxima gives the optical conductance of the sample. Phase shifts observable in the interference pattern of different graphene samples result from small differences in the substrate thickness of about 25 µm. The latter does not affect the amplitude of the patterns, that are all equal and 30% smaller than those for the empty substrate. By fitting the spectra with Equation 2, the graphene optical conductance G was obtained. The G values were corrected for the negligible but finite substrate absorption (Supporting Information).

To explore the effect of contaminants and Cu leftovers on the electronic quality of graphene, we measured the optical conductance G for different t_{etch} (Figure 3b) while keeping the PMMA layer on top (step 4 in Figure 1a). G is seen to increase monotonously with t_{etch} reaching a saturation value of $(2.3 \pm 0.1) \times 10^{-3}$ Ω^{-1} after 14 h. Moreover assuming a constant graphene Fermi velocity $\upsilon_F = 10^6$ m s^{-1}, illumination in the wavenumber range 26–35 cm^{-1} is expected to induce a lateral carrier displacement $l = \upsilon_F/\nu$ between 1.3 and 1 µm. Correspondingly, in order for an object to be nontransparent, its size must exceed ≈1 µm, which is well above the average size of molecular contaminants and Cu impurities already at $t_{etch} > 15$ min. This is further confirmed by the flat frequency behavior at lower wavenumbers (9–20 cm^{-1}) (Supporting Information). These observations show that Cu leftovers may contribute to the sample optical conductance only for very short t_{etch}, while for long t_{etch}, Cu residues behave as charged scatterers, possibly together with other contaminants, degrading the electronic quality of graphene.[40] Increasing t_{etch}, the amount of Cu impurities decreases and the electronic quality of pristine graphene is gradually approached. Upon removal of the PMMA layer (step 5 in Figure 1a), the optical conductance decreases sharply to $(1.0 \pm 0.1) \times 10^{-3}$ Ω^{-1} (Figure 3c). As PMMA is fully transparent at these frequencies and thicknesses, this difference reveals the doping effect of a higher-κ

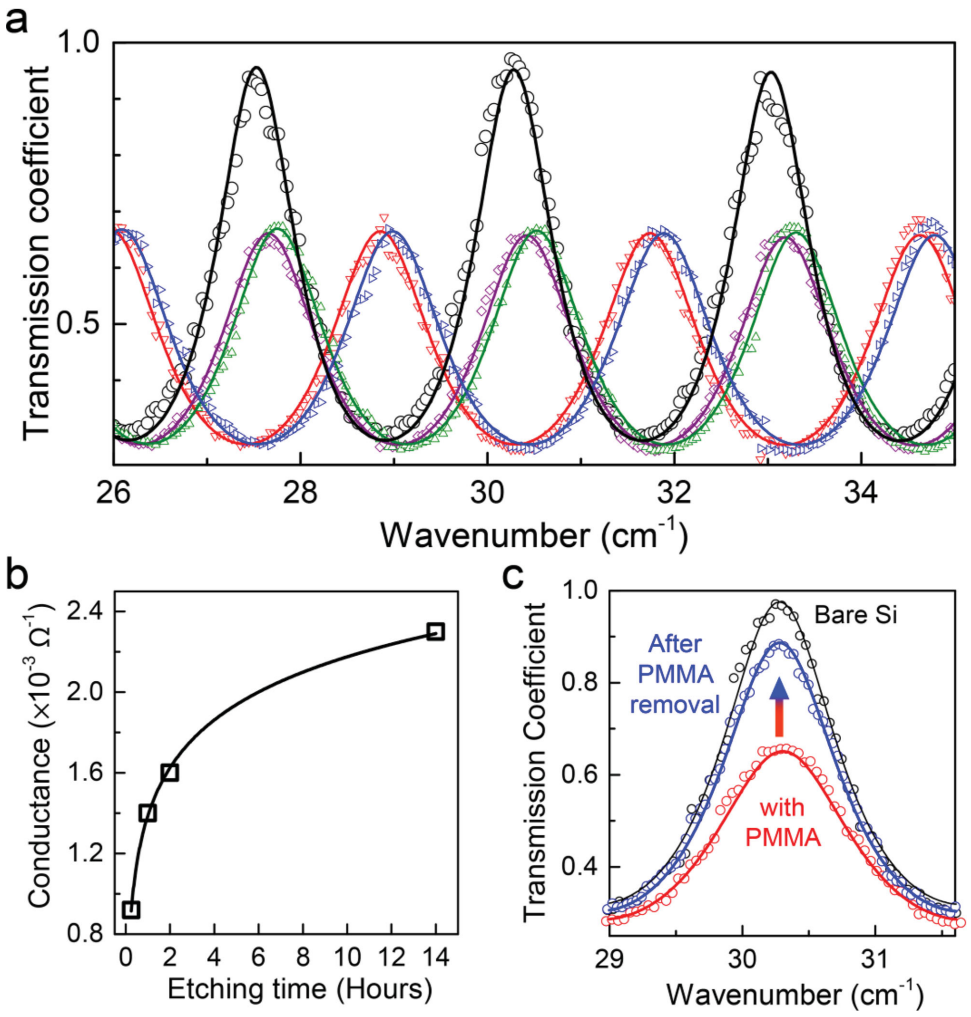

Figure 3. Effect of Cu and PMMA left-overs. a) Transmission spectra of a Si substrate without (black) and with (color) graphene/PMMA stack on top (t_{etch} = 14 h). Different colors indicate different samples. b) Conductivity of graphene for different Cu etching time. The line is a guide to the eye. c) Comparison of transmission amplitudes for graphene on Si, before (red) and after (blue) PMMA removal.

dielectric environment. Air has a relative permittivity almost half that of PMMA ($\kappa_{air} = 1$, $\kappa_{PMMA} \approx 2.6$); removal of the latter shifts the Fermi level closer to charge neutrality point, driving G toward the well-known conductance minimum.

The optical conductance of graphene is predicted to assume the universal value $G_0 = e^2/4\hbar = 6.1\times10^{-5}\,\Omega^{-1}$ (with e the electron charge and $\hbar$ Plank's constant) independent of frequency as an intrinsic property of massless Dirac fermions.[41,42] For the present bare graphene (without PMMA) samples, a much higher conductance of approximately $G \approx 30G_0$ is detected at the lowest frequency (**Figure 4**a). Similarly, large values have been observed at higher frequencies[19,29,42,43] and in time-resolved measurements[25,27] on large-area graphene. It is noteworthy that in contrast to previous works that use higher frequencies,[44] in our experiments the conductance is independent of the type of substrate (Supporting Information). The high value of $G \approx 30G_0$ suggests that the optical response of graphene at such low frequencies is notably affected by inhomogeneities and the finite temperature. In this context, it is relevant that the dc conductance minimum of graphene at the Dirac point[42] is governed by extrinsic factors, most prominently the presence of charged impurities on the substrate[45,46] and residual Cu. In the present case, the carrier scattering that arises from such impurities can be accounted for by the Drude model[38,39] and complementing the sub-THz measurements with higher-frequency absorption data gained by Fourier-transform spectroscopy. The combined frequency dependence, displayed in Figure 4a, is fitted with the Drude expression $\sigma(\nu) = \sigma_0\gamma^2/(\nu^2 + \gamma^2)$, where σ_0 is the DC conductivity and γ is the carrier scattering rate.[38,39] The value of γ was found to be 270 cm^{-1} at high temperature T, in agreement with previous reports.[28,29] The T dependence of γ, (Figure 4b) shows a T-independent contribution below 100 K and a marked increase at higher temperatures, indicating two different scattering contributions. The T-independent contribution is associated with defects and charged impurities and is the dominant factor limiting the conductance of graphene at low temperatures.[45–47] Fitting by a power dependence $T\beta$ yielded $\beta > 2$, which cannot be attributed to scattering by longitudinal graphene phonons as this mechanism would afford $\beta = 1$.[47] Instead, such strong temperature dependence

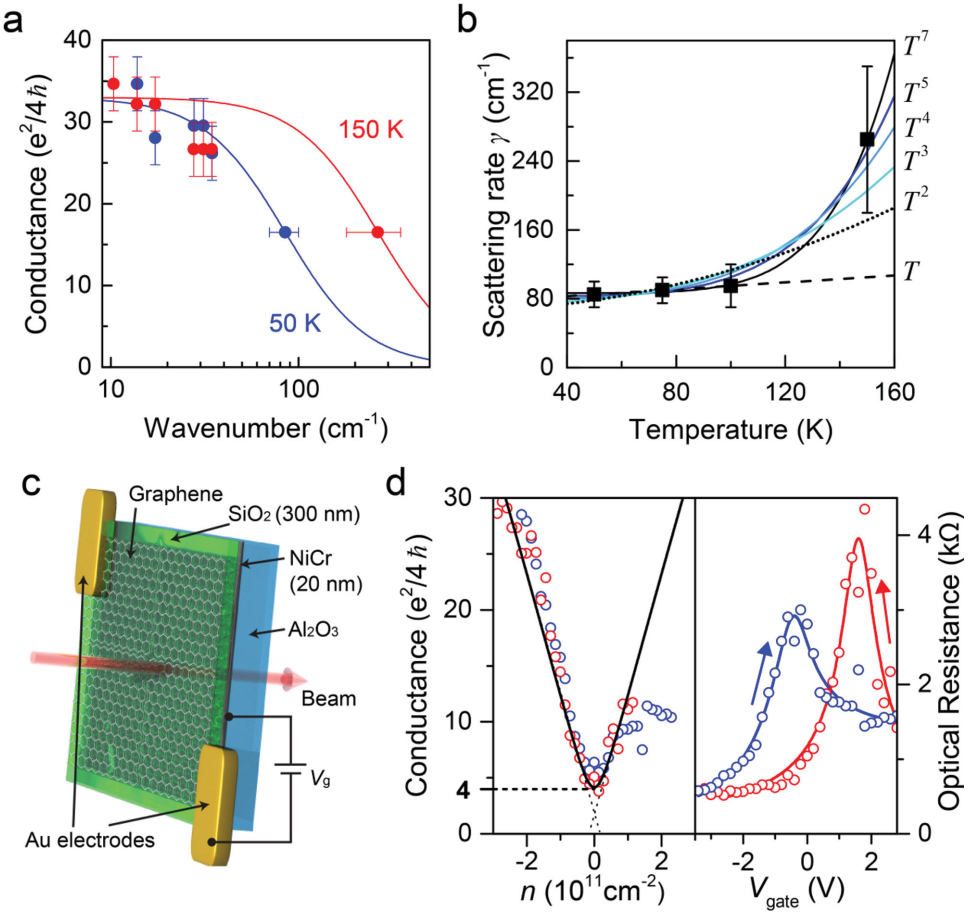

Figure 4. a) Frequency dependence of the graphene conductance at two different temperatures on Al_2O_3 substrate. The lines are fits using the Drude model. b) Temperature dependence of the carriers scattering rate, as extracted from the Drude fits. The solid line is a simulation of the T^{β} dependence for different β. $\beta > 1$ indicates electron–extrinsic phonons scattering. c) Structure of the THz-transparent multilayer structure for the optical characterization of the *n*-dependence of the conductance. d) Gate dependence of the optical behavior at 300 K recorded at 9 cm^{-1} (red and blue are different sweeps), showing: conductance versus *n* (left) and resistance versus V_g (right). The lines are fits to the data. The dashed black line indicates $4e^2/h$.

indicates scattering by substrate phonons to be the dominant mechanism limiting *G* at high temperatures.[48–50] The residual $\gamma = 86 \pm 1$ cm^{-1} corresponds[29] to a concentration of scatterers of $(3.4 \pm 0.5) \times 10^{11}$ cm^{-2}, in agreement with previous reports for CVD graphene[13,28] and comparable to typical exfoliated graphene flakes at room temperature.[2,51] The latter observation is a hint that grain boundaries do not represent the dominant source of scattering in these samples, as also suggested by transport measurements.[18]

With the aim of determining the carrier mobility and compensating for the residual doping, we introduced a gate that allows tuning the graphene charge density *n*. To maintain the transparency necessary for investigation at sub-THz energies, we fabricated the multilayer structure depicted in Figure 4c. It is composed of a Al_2O_3 substrate, a 20 nm-thick Ni:Cr alloy layer, with a d = 300 nm-thick e-gun-evaporated SiO_2 layer serving as gate dielectric on top of which the CVD graphene is transferred. The Ni:Cr alloy was chosen because it forms closed, electrically conducting thin films of sufficient high transparency in the sub-THz frequency range. The resulting device has an overall transmission coefficient of 0.15 in the 9–20 cm^{-1} range (Supporting Information). The gate voltage V_g is applied between graphene, contacted with Au/Cr contacts, and the Ni:Cr layer. The optical conductance at 9 cm^{-1} recorded as a function of gate voltage is shown in Figure 4d. The characteristic minimum at $V_g \neq 0$ indicates the Dirac point. Similar to dc electrical transport measurements, the V_g dependence exhibited hysteretic behavior under ambient conditions, owing to polar impurities and adsorbed water.[52] The *R* versus V_g curve reveals a pronounced electron–hole asymmetry at high carrier densities. As the present contactless technique is not affected by work-function mismatch at the electrical contacts like in dc transport studies,[54] it follows that in graphene charge impurities have different scattering cross-sections for electrons and holes.[53] Fitting with[55] $R(V_g) = R_S + \left(e\mu_c\sqrt{n_0^2 + n(V_g)^2}\right)^{-1}$ (R_S is the short-range scattering contribution to resistance, n_0 the residual carrier density at the charge-neutrality point due to electron–hole puddles[56] and $n = (\varepsilon_0\kappa_{SiO_2}/ed)V_g$ where ε_0 is the vacuum permittivity and $\kappa_{SiO_2} = 3.9$) yields a mobility of $\mu_e = (4.5 \pm 0.5) \times 10^4$ cm^2 V^{-1} s^{-1} for electrons and $\mu_h = (4.7 \pm 0.7) \times 10^4$ cm^2 V^{-1} s^{-1} for holes. The extracted mobilities are one to two orders of magnitude higher than those typically derived from dc measurements of CVD graphene on SiO_2,[1,15] while

they closely match those of clean exfoliated flakes[13] or single-grain CVD crystals.[14] This finding supports our conclusion that sub-THz optical detection probes the intrinsic conductance of the domains that constitute the CVD layer, consistent with the fact that at 9 cm^{-1} it induces electronic oscillations over lengths $l \approx 5$ µm, below the average domain size in CVD graphene. It follows that the observed mobilities are limited by surface-scatterers, analogous to other, solid-supported graphene sheets. Contact effects, which play a significant role in dc transport measurements,[54] certainly do not affect the conductance determined by optical means. Hence, the density of charged long-range scatterers can be estimated[45] close to the Dirac point. From the two branches of the curve, values of $(7 \pm 2) \times 10^{10}$ and $(9.5 \pm 1) \times 10^{10}$ cm^{-2} are extracted, which are only slightly lower than estimated above from the T-dependence of γ. Comparison with electrical transport experiments on large CVD surfaces indicates that crystal defects contribute a density of $\approx 10^2$ cm^{-2} to short range scattering. Importantly, the applied gate voltage allows compensating for the extrinsic doping by charged impurities, yielding a conductance of $G \approx 4G_0$, much lower than previously reported.[19,25,27] This provides further support that larger conductance values arise from extrinsic doping (i.e., Cu and molecular contaminants or surface charges).

In conclusion, by using contactless sub-THz interferometry, we could measure the electronic response of individual domains in wafer-sized CVD graphene. Using multilayer transparent structures we could observe the intrinsic optical conductance of graphene, as predicted by theoretical models. The mobility values observed are orders of magnitude higher than those obtained by transport measurements on equivalent CVD graphene,[1,15] reaching the same values of exfoliated graphene[1,51] or single CVD grains obtained with advanced techniques.[13,14] The mobility is found to be mainly limited by charged scatterers on the substrate, and our observations provide a validation of previous theoretical predictions.[45] The observed sensitivity of sub-THz interferometry to contaminants can be used to easily quantify their presence and assess the quality of large graphene structures, which is essential for applications in touchscreens, wearable, and optoelectronic devices.

Experimental Section

Etching Solution: A quantity of 8.4 g of $FeCl_3$ in 10 mL of 1:10 HCl water solution and further diluted in 50 mL of deionized water.

PMMA Removal Procedure: Four hours in hot (40 °C) acetone, 30 min in fresh 2-propanol, 15 min in 1,2-dichloroethane, and 15 min in 2-propanol.

Low-T Measurements: The sample was positioned in a cryostat equipped with Mylar windows.

Bilayer Graphene Stack for Grain Size Evaluation: Both graphene layers were etched for 14 h following the procedure of Figure 1a. In order to maximize the interlayer interaction, the sample was annealed in forming gas overnight at 400 °C after each graphene transfer.

Supporting Information

Supporting Information is available from the Wiley Online Library or from the author.

Acknowledgements

The authors acknowledge J. Winter for help with the sample fabrication, M. Scheffler and L. Duong for valuable discussions and financial support from German Deutsche Forschungsgemeinschaft, the Landesstiftung Baden-Württemberg (Kompetenznetz Funktionelle Nanostrukturen), the Alexander von Humboldt Stiftung (Sofja Kovalevskaja), International Max Planck Research School for Advanced Materials, EU ERC-StG-338258-"OptoQMol", the Royal Society (University Research Fellowship) and the Russian Ministry of education and science ("5 top 100" program).

Received: February 4, 2015
Published online: March 18, 2015

[1] A. K. Geim, K. S. Novoselov, *Nat. Mater.* **2007**, *6*, 183.
[2] K. S. Kim, Y. Zhao, H. Jang, S. Y. Lee, J. M. Kim, J. Ahn, P. Kim, J.-Y. Choi, B. H. Hong, *Nature* **2009**, *457*, 706.
[3] F. Bonaccorso, Z. Sun, T. Hasan, A. C. Ferrari, *Nat. Photonics* **2010**, *4*, 611.
[4] W. Yang, K. R. Ratinac, S. P. Ringer, P. Thordarson, J. J. Gooding, F. Braet, *Angew. Chem. Int. Ed.* **2010**, *49*, 2114.
[5] W. Han, R. K. Kawakami, M. Gmitra, J. Fabian, *Nat. Nanotechnol.* **2014**, *9*, 794.
[6] G. Eda, G. Fanchini, M. Chhowalla, *Nat. Nanotechnol.* **2008**, *3*, 270.
[7] A. Reina, X. Jia, J. Ho, D. Nezich, H. Son, V. Bulovic, M. S. Dresselhaus, J. Kong, *Nano Lett.* **2009**, *9*, 30.
[8] X. Wang, L. Zhi, K. Müllen, *Nano Lett.* **2008**, *8*, 323.
[9] O. V. Yazyev, S. G. Louie, *Nat. Mater.* **2010**, *9*, 806.
[10] A. W. Tsen, L. Brown, M. P. Levendorf, F. Ghahari, P. Y. Huang, R. W. Havener, C. S. Ruiz-Vargas, D. A. Muller, P. Kim, J. Park, *Science* **2012**, *336*, 1143.
[11] J. Lahiri, Y. Lin, P. Bozkurt, I. I. Oleynik, M. Batzill, *Nat. Nanotechnol.* **2010**, *5*, 326.
[12] G.-X. Ni, Y. Zheng, S. Bae, H. R. Kim, A. Pachoud, Y. S. Kim, C.-L. Tan, D. Im, J.-H. Ahn, B. H. Hong, B. Özyilmaz, *ACS Nano* **2012**, *6*, 1158.
[13] X. Li, W. Cai, J. An, S. Kim, J. Nah, D. Yang, R. Piner, A. Velamakanni, I. Jung, E. Tutuc, S. K. Banerjee, L. Colombo, R. S. Ruoff, *Science* **2009**, *324*, 1312.
[14] N. Petrone, C. R. Dean, I. Meric, A. M. Van Der Zande, P. Y. Huang, L. Wang, D. Muller, K. L. Shepard, J. Hone, *Nano Lett.* **2012**, *12*, 2751.
[15] X. Li, C. W. Magnuson, A. Venugopal, J. An, J. W. Suk, B. Han, M. Borysiak, W. Cai, A. Velamakanni, Y. Zhu, L. Fu, E. M. Vogel, E. Voelkl, L. Colombo, R. S. Ruoff, *Nano Lett.* **2010**, *10*, 4328.
[16] S. Bae, H. R. Kim, Y. Lee, X. Xu, J.-S. Park, Y. Zheng, J. Balakrishnan, T. Lei, H. R. Kim, Y. I. Song, Y.-J. Kim, K. S. Kim, B. Ozyilmaz, J.-H. Ahn, B. H. Hong, S. Iijima, *Nat. Nanotechnol.* **2010**, *5*, 574.
[17] X. Liang, B. B. A. Sperling, I. Calizo, G. Cheng, C. A. Hacker, Q. Zhang, Y. Obeng, K. Yan, H. Peng, Q. Li, X. Zhu, H. Yuan, A. R. Hight Walker, Z. Liu, L. Peng, C. A. Richter, *ACS Nano* **2011**, *5*, 9144.
[18] P. Y. Huang, C. S. Ruiz-Vargas, A. M. van der Zande, W. S. Whitney, M. P. Levendorf, J. W. Kevek, S. Garg, J. S. Alden, C. J. Hustedt, Y. Zhu, J. Park, P. L. McEuen, D. Muller, *Nature* **2011**, *469*, 389.
[19] J. Horng, C.-F. Chen, B. Geng, C. Girit, Y. Zhang, Z. Hao, H. A. Bechtel, M. Martin, A. Zettl, M. F. Crommie, Y. R. Shen, F. Wang, *Phys. Rev. B* **2011**, *83*, 165113.
[20] K. Pi, K. M. McCreary, W. Bao, W. Han, Y. F. Chiang, Y. Li, S.-W. Tsai, C. N. Lau, R. K. Kawakami, *Phys. Rev. B* **2009**,*80*, 75406.
[21] C. J. Docherty, M. B. Johnston, *J. Infrared, Millimeter, Terahertz Waves* **2012**, *33*, 797.

[22] G. Jnawali, Y. Rao, H. Yan, T. F. Heinz, *Nano Lett.* **2013**, *13*, 524.
[23] S.-F. Shi, T.-T. Tang, B. Zeng, L. Ju, Q. Zhou, A. Zettl, F. Wang, *Nano Lett.* **2014**, *14*, 1578.
[24] A. J. Frenzel, C. H. Lui, W. Fang, N. L. Nair, P. K. Herring, P. Jarillo-Herrero, J. Kong, N. Gedik, *Appl. Phys. Lett.* **2013**, *102*, 113111.
[25] J. L. Tomaino, A. D. Jameson, J. W. Kevek, M. J. Paul, A. M. van der Zande, R. A. Barton, P. L. McEuen, E. D. Minot, Y.-S. Lee, *Opt. Express* **2011**, *19*, 141.
[26] I. Maeng, S. Lim, S. J. Chae, Y. H. Lee, H. Choi, J.-H. Son, *Nano Lett.* **2012**, *12*, 551.
[27] L. Ren, Q. Zhang, J. Yao, Z. Sun, R. Kaneko, Z. Yan, S. Nanot, Z. Jin, I. Kawayama, M. Tonouchi, J. M. Tour, J. Kono, *Nano Lett.* **2012**, *12*, 3711.
[28] Z. Q. Li, E. A. Henriksen, Z. Jiang, Z. Hao, M. C. Martin, P. Kim, H. L. Stormer, D. N. Basov , *Nat. Phys.* **2008**, *4*, 532.
[29] H. Yan, F. Xia, W. Zhu, M. Freitag, C. Dimitrakopoulos, A. A. Bol, G. Tulevski, P. Avouris, *ACS Nano* **2011**, *5*, 9854.
[30] J. Y. Kim, C. Lee, S. Bae, K. S. Kim, B. H. Hong, *Appl. Phys. Lett.* **2011**, *98*, 201907.
[31] C. J. Docherty, C.-T. Lin, H. J. Joyce, R. J. Nicholas, L. M. Herz, L.-J. Li, M. B. Johnston, *Nat. Commun.* **2012**, *3*, 1228.
[32] F. Liu, Y. D. Chong, S. Adam, M. Polini, *2D Mater.* **2014**, *1*, 031001.
[33] A. C. Ferrari, J. C. Meyer, V. Scardaci, C. Casiraghi, M. Lazzeri, F. Mauri, S. Piscanec, D. Jiang, K. S. Novoselov, S. Roth, A. K. Geim, *Phys. Rev. Lett.* **2006**, *97*, 187401.
[34] C. Casiraghi, S. Pisana, K. S. Novoselov, A. K. Geim, A. C. Ferrari, *Appl. Phys. Lett.* **2007**, *91*, 233108.
[35] Q. H. Wang, Z. Jin, K. K. Kim, A. J. Hilmer, G. L. C. Paulus, C.-J. Shih, M.-H. Ham, J. D. Sanchez-Yamagishi, K. Watanabe, T. Taniguchi, J. Kong, P. Jarillo-Herrero, M. S. Strano, *Nat. Chem.* **2012**, *4*, 724.
[36] S. D. Costa, A. Righi, C. Fantini, Y. Hao, C. Magnuson, L. Colombo, R. S. Ruoff, M. A. Pimenta, *Solid State Commun.* **2012**, *152*, 1317.
[37] R. W. Havener, H. Zhuang, L. Brown, R. G. Henning, J. Park, *Nano Lett.* **2012**, *12*, 3162.
[38] B. Gorshunov, A. Volkov, I. Spektor, A. Prokhorov, A. Mukhin, M. Dressel, S. Uchida, A. Loidl, *Int. J. Infrared Millimeter Waves* **2005**, *26*, 1217.
[39] U. S. Pracht, E. Heintze, C. Clauss, D. Hafner, R. Bek, D. Werner, S. Gelhorn, M. Scheffler, M. Dressel, D. Sherman, B. Gorshunov, K. S. Il'In, D. Henrich, M. Siegel, *IEEE Trans. Terahertz Sci. Technol.* **2013**, *3*, 269.
[40] a) A. V. Kretinin, Y. Cao, J. S. Tu, G. L. Yu, R. Jalil, K. S. Novoselov, S. J. Haigh, A. Gholinia, A. Mishchenko, M. Lozada, T. Georgiou, C. R. Woods, F. Withers, P. Blake, G. Eda, A. Wirsig, C. Hucho, K. Watanabe, T. Taniguchi, A. K. Geim, R. V. Gorbachev, *Nano Lett.* **2014**, *14*, 3270; b) K. Pi, W. Han, K. M. McCreary, A. G. Swartz, Y. Li, R. K. Kawakami, *Phys. Rev. Lett.* **2010**, *104*, 187201; c) K. Pi, K. M. McCreary, W. Bao, W. Han, Y. F. Chiang, Y. Li, S.-W. Tsai, C. N. Lau, R. K. Kawakami, *Phys. Rev. B* **2009**, *80*, 75406.
[41] a) E. G. Mishchenko, *Phys. Rev. Lett.* **2007**, *98*, 216801; b) T. Stauber, N. M. R. Peres, A. H. Castro Neto, *Phys. Rev. B* **2008**, *78*, 85418.
[42] R. R. Nair, P. Blake, N. Grigorenko, K. S. Novoselov, T. J. Booth, T. Stauber, N. M. R. Peres, A K. Geim, *Science* **2008**, *320*, 1308.
[43] K. F. Mak, M. Y. Sfeir, Y. Wu, C. H. Lui, J. A. Misewich, T. F. Heinz, *Phys. Rev. Lett.* **2008**, *101*, 196405.
[44] B. Scharf, V. Perebeinos, J. Fabian, P. Avouris, *Phys. Rev. B* **2013**, *87*, 035414.
[45] S. Adam, E. H. Hwang, V. M. Galitski, S. Das Sarma, *Proc. Natl. Acad. Sci. USA* **2007**, *104*, 18392.
[46] S. V. Morozov, K. S. Novoselov, M. I. Katsnelson, F. Schedin, D. C. Elias, J. A. Jaszczak, A. K. Geim, *Phys. Rev. Lett.* **2008**, *100*, 16602.
[47] E. Hwang, S. Das Sarma, *Phys. Rev. B* **2009**, *79*, 165404.
[48] E. V. Castro, H. Ochoa, M. I. Katsnelson, R. V. Gorbachev, D. C. Elias, K. S. Novoselov, A. K. Geim, F. Guinea, *Phys. Rev. Lett.* **2010**, *105*, 266601.
[49] E. H. Hwang, S. Das Sarma, *Phys. Rev. B* **2008**, *77*, 115449.
[50] E. Mariani, F. von Oppen, *Phys. Rev. B* **2010**, *82*, 195403.
[51] K. S. Novoselov, A. K. Geim, S. V Morozov, D. Jiang, I. V. Grigorieva, S. V. Dubonos, A. A. Firsov, *Nature* **2005**, *438*, 197.
[52] W. Kim, A. Javey, O. Vermesh, Q. Wang, Y. Li, H. Dai, *Nano Lett.* **2003**, *3*, 193.
[53] D. S. Novikov, *Appl. Phys. Lett.* **2007**, *91*, 102102.
[54] B. Huard, N. Stander, J. A. Sulpizio, D. Goldhaber-Gordon, *Phys. Rev. B* **2008**, *78*, 121402.
[55] S. Kim, J. Nah, I. Jo, D. Shahrjerdi, L. Colombo, Z. Yao, E. Tutuc, S. K. Banerjee, *Appl. Phys. Lett.* **2009**, *94*, 62107.
[56] J. Martin, N. Akerman, G. Ulbricht, T. Lohmann, J. H. Smet, K. von Klitzing, A. Yacoby, *Nat. Phys.* **2008**, *4*, 144.